RSC Advances

PAPER

View Article Online
View Journal | View Issue

Cite this: *RSC Adv.*, 2019, **9**, 24811

Functionalization of theranostic AGuIX® nanoparticles for PET/MRI/optical imaging†

Vivek Thakare,[ab] Vu-Long Tran,[cd] Marco Natuzzi,[c] Eloïse Thomas,[c] Mathieu Moreau,[a] Anthony Romieu,[ae] Bertrand Collin,[af] Alan Courteau,[f] Jean-Marc Vrigneaud,[f] Cédric Louis,[d] Stéphane Roux,[g] Frédéric Boschetti,[b] Olivier Tillement,[ch] François Lux[ch] and Franck Denat*[a]

Received 15th January 2019
Accepted 1st August 2019

DOI: 10.1039/c9ra00365g

rsc.li/rsc-advances

A novel trifunctional imaging probe containing a chelator of radiometal for PET, a NIR heptamethine cyanine dye, and a bioconjugatable handle, has been grafted onto AGuIX® nanoparticles *via* a Michael addition reaction. The resulting functionalized nanoparticles have been fully characterized, radiolabelled with ^{64}Cu, and evaluated in a mice TSA tumor model using multimodal (PET/MRI/optical) imaging.

The design of multi-modal contrast agents has become one of the thrust areas of research in molecular imaging science.[1,2] Combination of two imaging modalities can be really advantageous if they complement each other in revealing the correct biological information for preclinical and clinical use. This approach has given rise to hybrid imaging modalities like PET/MRI, SPECT or PET/CT, or PET/OI. Hybrid imaging helps in retrieving the information that otherwise would not be available with individual modality. For instance, the combination of functional information (from PET) and anatomic/spatial information (obtained by CT or MRI) into a single image provides a more accurate diagnostic.[3,4] Combining nuclear and optical imaging also represents a valuable approach.[5–7] Indeed, PET or SPECT whole-body scan may allow diagnosis and staging of patients, whereas optical imaging can be used for intra-operative surgical assistance. To successfully leverage such symbiosis, it is necessary to develop tracers that can have dual/multiple functionality. Nanoparticles represent a class of materials that are well suited to such purpose as they exhibit intrinsic imaging and/or therapeutic properties and they can be easily functionalized to add other modalities.[8–10] Among promising nanomaterials, AGuIX® are particularly attractive. These sub-5 nm nanoparticles, firstly described in 2011,[11] are composed of a polysiloxane matrix on which DOTAGA–Gd complexes are covalently bound. AGuIX® nanoparticles have already shown their therapeutic efficiency as radiosensitizers on different *in vivo* preclinical models of cancer: glioblastoma, brain metastases, melanoma, pancreatic cancer, liver cancer, head and neck cancer and lung cancer.[12] They have been recently translated to the clinic, for the treatment of multiple brain metastases and for cervix cancer in association with radiation therapy.[12] New generations of AGuIX® nanoparticles have been developed by functionalization of their surface, for example by addition of ^{68}Ga[13] or ^{89}Zr[14] chelators for PET/MRI imaging.

Here we report a method for the dual functionalization of AGuIX® nanoparticles with both a macrocyclic chelator optimized for the complexation of a PET radioisotope (^{64}Cu or ^{68}Ga) and a NIR heptamethine cyanine dye. Owing to the intrinsic properties of the pristine AGuIX® nanoparticles, the resulting nano-object is a theranostic nanoparticle that can be tracked *in vivo* using three different imaging modalities, *i.e.*, PET, MR and optical imaging. Our strategy relies on the use of a monomolecular multimodal imaging probe (MOMIP) which contains within one single molecule: (i) a chelating agent (in this case a NODAGA moiety which has become in the last years a chelator of choice for ^{64}Cu and ^{68}Ga),[15,16] (ii) a Cy-7 derivative (known as IR-783, and bearing a reactive *meso*-chlorine atom),[17,18] (iii) a reactive handle for grafting the MOMIP to the surface of the nanoparticles (here a maleimide group). The use of such MOMIP for appending different imaging reporters to the nanoparticle is highly beneficial when compared to the sequential grafting of the two different probes, which can present many process and characterization related challenges. Indeed, our approach allows a better control of the chemical

[a]*Institut de Chimie Moléculaire de l'Université de Bourg, UMR 6302, CNRS, Université Bourgogne Franche-Comté, 9 Avenue Alain Savary, 21000, Dijon, France. E-mail: franck.denat@u-bourgogne.fr*

[b]*CheMatech, 2 rue Pauline Kergomard, 21000, Dijon, France*

[c]*Univ Lyon, Université Claude Bernard Lyon 1, CNRS, Institut Lumière Matière, F-69622, Lyon, France*

[d]*Nano H SAS, 2 Place de l'Europe, 38070 Saint Quentin Fallavier, France*

[e]*Institut Universitaire de France, 1, Rue Descartes, Bâtiment MONGE, 75231 Paris, France*

[f]*Georges-François LECLERC Cancer Center – UNICANCER, 1 rue Pr Marion, 21079, Dijon, France*

[g]*Institut UTINAM, UMR6213, CNRS, Université de Bourgogne Franche-Comté, 16 route de Gray, 25030, Besançon, France*

[h]*NH TherAguix SAS, F69100 Villeurbanne, France*

† Electronic supplementary information (ESI) available. See DOI: 10.1039/c9ra00365g

composition of the resulting nano-objects, in particular the ratio of the two probes, and enables a better reproducibility of the synthesis. Several MOMIP containing BODIPY and DOTA derivatives have been developed by our group and conjugated to various biomolecules such as peptides,[19] monoclonal antibodies,[20] or lipopolysaccharides,[21] providing proofs of concept of such strategy for dual SPECT/optical imaging.

The development of the desired MOMIP entails a multistep chemical synthesis with series of coupling and deprotection steps. In a typical MOMIP synthesis, the bioconjugatable handle is introduced at the last step, because of its sensitivity and reactivity. In the synthetic strategy described herein, we also wanted to consider if it was possible to introduce more stable functions such as maleimide earlier, and in particular in the first step of the synthesis. This strategy is particularly valuable when working with sensitive fluorophores such as polymethine cyanine dyes which could then be introduced in the very last step. This approach was successful, and the MOMIP IR-783-Lys(Mal)NODAGA (**6**) could be obtained as depicted in Fig. 1A. The lysine derivative **1**, obtained almost quantitatively by coupling 6-maleimidohexanoic acid to the commercially available Boc-Lys-OH was linked to the bifunctional chelating agent **2** *via* the intermediate *N*-hydroxysuccinimidyl (NHS) ester formation, yielding compound **3** in 55% yield. Compound **4** was then obtained by single step deprotection of both the *tert*-butyl ester and Boc protecting groups of chelator and lysine units, using TFA. The final MOMIP IR-783-Lys(Mal)NODAGA (**6**) could be synthesized *via* the amide coupling of **4** and dye **5**, easily obtained through nucleophilic substitution of the chlorine atom at the *meso* position of IR-783 by 6-mercaptohexanoic acid.

The surface of the AGuIX® nanoparticles possesses primary amino groups that stem from the APTES (3-aminopropyltriethoxysilane) reagent that is used in the synthetic process. In order to generate thiol groups at the surface of the nanoparticles, able to react with the maleimide moiety of the MOMIP **6**, nanoparticles were thiolated with Traut's reagent at pH 8 for 1 h (Fig. 1B). After purification by ultrafiltration cycles, the sulfhydryl-functionalized AGuIX® nanoparticles were characterized by Ellman's assay to determine the number of thiol groups appended, which was found to be around 2.5 per nanoparticle. This degree of thiolation was considered optimal for further conjugation as excessive thiolation might potentially cause nanoparticles to clump by inter-particulate disulfide bridging. The purified thiolated nanoparticles were immediately treated with the MOMIP **6** at pH 7, at room temperature and protected from light. In these conditions, the thiol–maleimide coupling proceeded quickly to form a stable thioether linkage.

The functionalized AGuIX-NODAGA-IR783 nanoparticles were characterized using various analytical techniques (Table 1). Their hydrodynamic diameter D_h was measured using Dynamic Light Scattering (DLS). The size of the pristine AGuIX® nanoparticles was found to be 4.6 ± 0.9 nm whereas the thiolated nanoparticles exhibited a similar size. Upon grafting of the macromolecular probe, the D_h of nanoparticles increased to 12.1 ± 3.0 nm due to the bulky nature of the bimodal probe but the nanoparticles remain small enough to be eliminated mainly through the kidneys. Relaxometric measurements revealed that r_1 and r_2 increased significantly upon functionalization due to an increase of the rotational correlation time resulting from the grafting of the MOMIP. The ratio r_2/r_1 is consistent with the use of these nanoparticles as a positive MRI contrast agent. The relative content of Gd reduces considerably and this is reasonable given the high molecular weight of the MOMIP.

The functionalized nanoparticles were very readily dispersible in PBS and photophysical measurements were performed (Fig. S2†). The absorption and emission maxima are centered at 792 nm and 815 nm respectively. Molar extinction coefficient of bound Cy-7 chromophore could not be calculated as the functionalized nanoparticles represent a complex macromolecular structure without any assignable molecular weight. The dual absorption, the breadth of the absorption bands and the hypsochromic shift of one band to 725 nm is consistent with the formation of non-emissive aggregates (H-type aggregates) promoted by inter-nanoparticles interactions. Consequently, the relative fluorescence quantum yield $\Phi_F = 0.4\%$ (determined

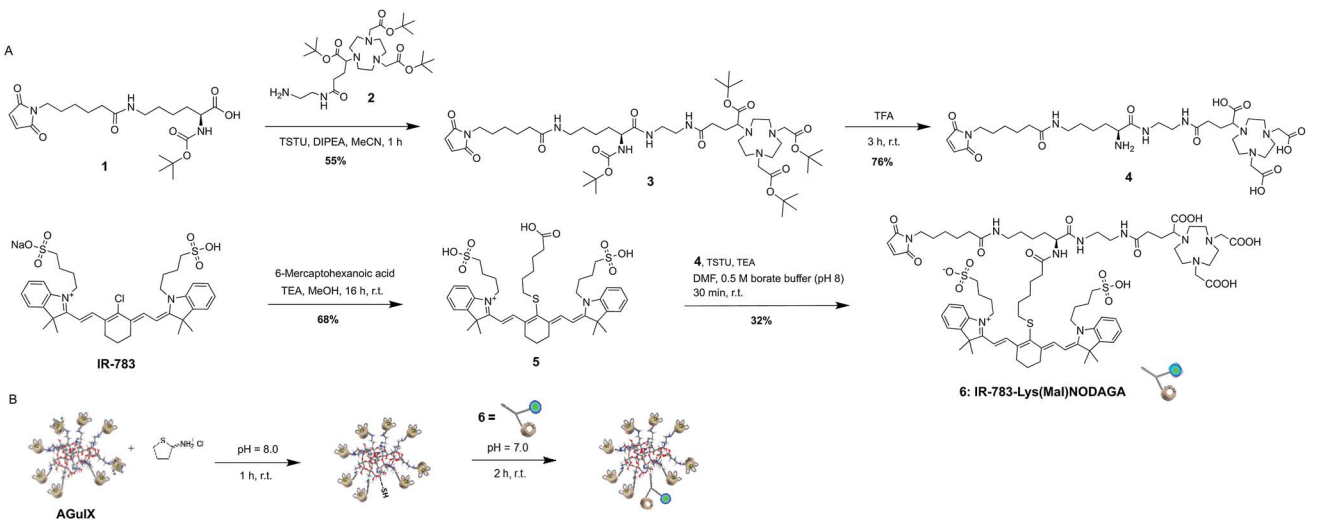

Fig. 1 (A) Synthesis of MOMIP IR-783-Lys(Mal)NODAGA **6**. (B) Functionalization of AGuIX® with MOMIP **6**.

Table 1 Physico-chemical characteristics of the nanoparticles

Feature	Method	AGuIX	AGuIX-SH	AGuIX-NODAGA-IR783
D_h (nm)	DLS	4.6 ± 0.9	4.5 ± 0.9	12.1 ± 3.0
Relative SH content	Ellman's assay	—	Gd : SH ∼ 10 : 2	—
r_1 (mM^{-1} s^{-1})	Relaxometry	13.5	16.8	16.9
r_2/r_1		1.35	1.39	1.83
Retention time (min)	HPLC	13.4	—	18
Purity (%)		80		95
Gd content (μmol mg^{-1})	ICP-OES	0.89	—	0.32

using ICG as standard, Φ_F = 10.6% in DMSO[22]) is modest. Nonetheless, these functionalized nanoparticles have photophysical similarities to ICG, their overall functional properties were not affected after functionalization, making them valuable candidates for imaging.

The next step was to study the feasibility of the radiolabelling of AGuIX-NODAGA-IR783 with ^{64}Cu. This radioisotope has been chosen because its decay characteristics ($t_{1/2}$ = 12.7 hours; β^+, 0.653 MeV [17.8%]) are well suited for PET imaging studies.[23] The functionalized nanoparticles were dispersed in NH_4OAc buffer (pH 5.5) and incubated with $^{64}CuCl_2$ at 37 °C for 45 min. The radiochemical purity of the radiolabelled nanoparticles was found to be >95% as determined by ITLC using 0.1 M EDTA as the mobile phase (Fig. S3†). Furthermore, stability investigations at 37 °C in human plasma and EDTA (EDTA challenge) revealed that the radiolabelled nanoparticles are stable over a period of 48 h as can be seen in Fig. 2. This evaluation at *in vitro* stage is very important to assess the ability of the nanoparticles to retain the radioisotope incorporated into it. Moreover, it is also reflective of the stability of radiolabelled nanoparticles in physiological conditions before proceeding to *in vivo* experiments.

Ultrasmall nanoparticles like AGuIX® are well suited for imaging applications owing to their fast tumor accumulation and renal clearance.[24,25] We report for the first time the development of such nanoparticles for simultaneous PET-MRI and optical trimodal imaging, which has been investigated in a TSA tumor model.‡ This can be of high value for intra-operative surgical guidance. PET-MRI images yielded information about the global distribution of these nanoparticles as can be seen from the improved MRI contrast and bright PET signals (Fig. 3A–C). The substantial decrease of the bright signals from the kidneys and the bladder from 1 h to 24 h, signifies potential renal excretion of the AGuIX-NODAGA-IR783 (^{64}Cu) nanoparticles. These observations were in line with the biodistribution data (Fig. 3D). Tumor to non tumor ratios (Fig. 3E) highlight a low but significant tumor uptake.

Unlike the pristine AGuIX® nanoparticles that are almost exclusively eliminated by renal way,[26] AGuIX-NODAGA-IR783 (^{64}Cu) nanoparticles accumulate to certain extent in liver and this can be ascribed to the hepatic uptake owing to the presence of IR-783 dye (ICG like dye show higher hepatic uptake and clearance)[27] and the increase of hydrodynamic diameter that is usually associated with accumulation in spleen and liver.[28] Hepatic clearance could be the additional mode of excretion along with renal pathway.

Accumulation of the nanoparticles in tumor appears to be moderate based on the biodistribution data, as against the stark signals with the optical imaging, which can be explained by higher sensitivity of the fluorescence at the tissue surface.[29] Indeed, owing to the sensitivity of the NIR fluorescent probes, the localization of the AGuIX-NODAGA-IR783 (^{64}Cu) into tumors could be easily traced (Fig. 4 left). After dissection, it appeared that the biodistribution observed is very different from PET-MRI images and gamma counting biodistribution, with a strong fluorescence signal in stomach and intestines (Fig. 4, right). Considering the large amount of AGuIX-NODAGA-IR783 (^{64}Cu) injected, it appears that the low signal in liver and kidneys is attributed to IR783 self-quenching due to the high concentration of the fluorescent dye in those organs. This has been confirmed by comparing the radiant efficiency of the nanoparticles at different concentrations (Fig. S4†). Consequently, organs with poor uptake give the highest radiant efficiency and a bright signal.

Nonetheless, these imaging studies clearly highlight the potential of such probes in multi-modal imaging along with their favorable clearance.

In summary, the synthesis of a trifunctional imaging probe was achieved through appropriate selection of linker/conjugation system, chelator for PET imaging and NIR fluorophore, and strategic synthetic schemes. This MOMIP has been successfully used for functionalization of AGuIX® nanoparticles. The functionalized nanoparticles have been thoroughly characterized for their physico-chemical attributes

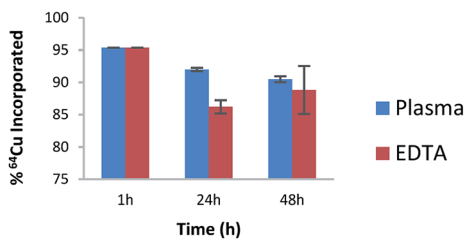

Fig. 2 Stability of AGuIX-NODAGA-IR783 (^{64}Cu) in plasma (blue) and upon EDTA challenge (red).

‡ The animal study was conducted in accordance with the legislation on the use of laboratory animals (directive 2010/63/EU) and was approved by accredited Ethical committee (C2ea Grand Campus no.105) and the French Ministries of Research (project #9617) and Agriculture (A 21 231 016 EA).

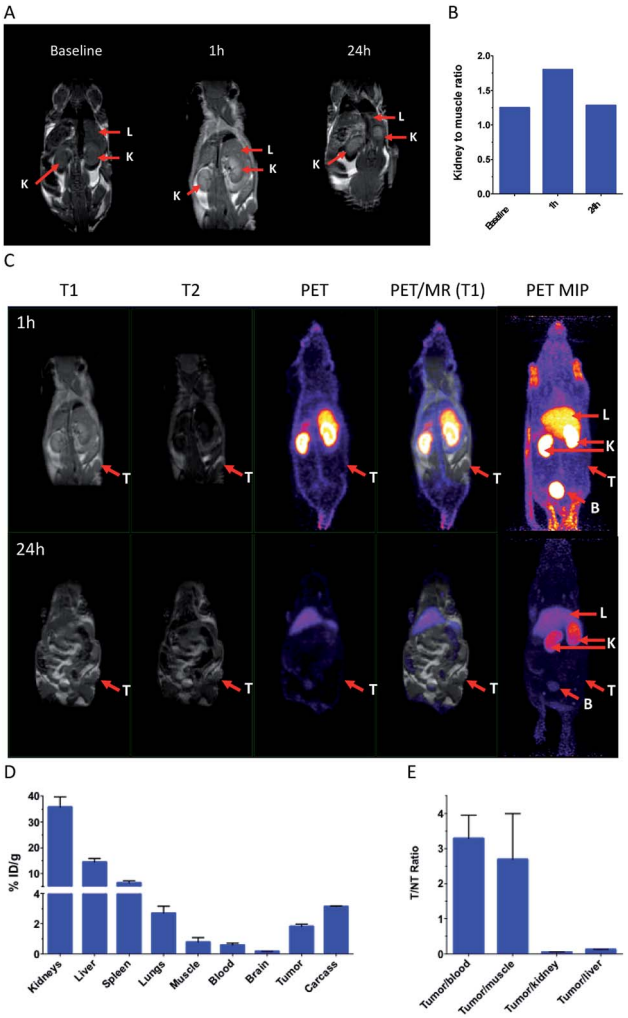

Fig. 3 (A) T1 MRI images in TSA tumor model. Coronal slice centered on kidneys (K) and liver (L) prior, 1 h and 24 h post-injection. (B) Kidney to muscle ratio prior, 1 h and 24 h post-injection. (C) PET-MRI images 1 h (top) and 24 h (bottom) post injection (T = tumor, K = kidneys, B = bladder and L = liver). MIP stands for Maximum Intensity Projection. (D) Biodistribution of AGuIX-NODAGA-IR783 (^{64}Cu) 24 h post injection. (E) Tumor to non-tumor ratio 24 h post injection.

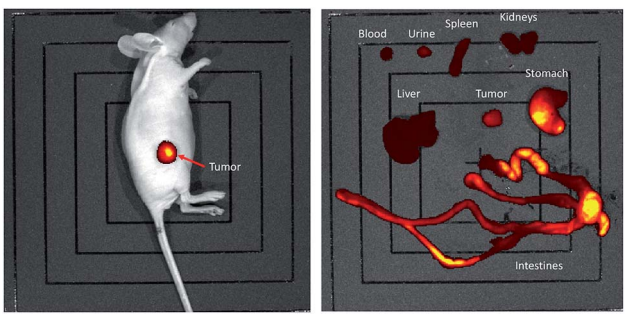

Fig. 4 Optical imaging in TSA tumor model 24 h (left) post-injection and after dissection (right).

relevant for imaging. These nanoparticles were radiolabelled with ^{64}Cu and were found to be stable under physiological conditions. These multifunctional nanoparticles were evaluated in TSA tumor model using PET-MRI-optical imaging, highlighting their favorable *in vivo* behavior. Above findings clearly demonstrate the usefulness of such approach for the development of sophisticated multimodal theranostic nanoparticles.

Ethical statement

All animal studies were conducted in accordance with the legislation on the use of laboratory animals (directive 2010/63/EU) and were approved by accredited Ethical committee (C2ea Grand Campus no. 105).

Conflicts of interest

FD is scientific advisor and shareholder of Chematech. FL and OT have to disclose the patent WO2011/135101. This patent protects the AGuIX® NPs described in this publication. FL and OT are employees from NH TherAguix that is developing the AGuIX® NPs and possess shares of this company.

Acknowledgements

The authors gratefully acknowledge the CNRS, the ''Université de Bourgogne'' and the European Union FP7-PEOPLE Initial Training Network ARGENT (Advanced Radiotherapy, Generated by Exploiting Nanoprocesses and Technologies) Project ID 608163 for the financial support. This work has also been supported by a French Government Grant managed by the French National Research Agency (ANR) under the program "Investissements d'Avenir" (reference ANR-10-EQPX-05-01/IMAPPI Equipex). AR thanks Institut Universitaire de France (IUF, 2013-2018) for financial support. This work is also part of the project "Pharmaco-imagerie et agents théranostiques" supported by the Conseil Régional de Bourgogne Franche-Comté through the « Plan d'Action Régional pour l'Innovation » (PARI) and by the European Union through the PO FEDER-FSE 2014/2020 Bourgogne program. This work was performed within Pharm'image, a regional centre of excellence in Pharmaco-imaging and within the GDR CNRS 2037 AIM (Molecular Imaging Agents).

Notes and references

1 L. E. Jennings and N. J. Long, *Chem. Commun.*, 2009, 3511–3524.
2 A. Louie, *Chem. Rev.*, 2010, **110**, 3146–3195.
3 H. Zaidi, O. Mawlawi and C. G. Orton, *Med. Phys.*, 2007, **34**, 1525–1528.
4 B. J. Pichler, M. S. Judenhofer and C. Pfannenberg, *Handb. Exp. Pharmacol.*, 2008, **185**, 109–132.
5 U. Seibold, B. Wängler, R. Schirrmacher and C. Wängler, *BioMed Res. Int.*, 2014, **2014**, 153741.
6 J. Culver, W. Akers and S. Achilefu, *J. Nucl. Med.*, 2008, **49**, 169–172.
7 F. L. Thorp-Greenwood and M. P. Coogan, *Dalton Trans.*, 2011, **40**, 6129–6143.

8 B. P. Burke, C. Cawthorne and S. J. Archibald, *Philos. Trans. R. Soc., A*, 2017, **375**, 20170261.
9 X. Li, X.-N. Zhang, X.-D. Li and J. Chang, *Cancer Biol. Med.*, 2016, **13**, 339–348.
10 E. Huynh and G. Zheng, *Wiley Interdiscip. Rev.: Nanomed. Nanobiotechnol.*, 2013, **5**, 250–265.
11 F. Lux, A. Mignot, P. Mowat, C. Louis, S. Dufort, C. Bernhard, F. Denat, F. Boschetti, C. Brunet, R. Antoine, P. Dugourd, S. Laurent, L. Vander Elst, R. Muller, L. Sancey, V. Josserand, J.-L. Coll, V. Stupar, E. Barbier, C. Rémy, A. Broisat, C. Ghezzi, G. Le Duc, S. Roux, P. Perriat and O. Tillement, *Angew. Chem., Int. Ed.*, 2011, **51**, 12299–13303.
12 F. Lux, V. L. Tran, E. Thomas, S. Dufort, F. Rossetti, M. Martini, C. Truillet, T. Doussineau, G. Bort, F. Denat, F. Boschetti, G. Angelovski, A. Detappe, Y. Crémillieux, N. Mignet, B.-T. Doan, B. Larrat, S. Meriaux, E. Barbier, S. Roux, P. Fries, A. Müller, M.-C. Abadjian, C. Anderson, E. Canet-Soulas, P. Bouziotis, M. Barberi-Heyob, C. Frochot, C. Verry, J. Balosso, M. Evans, J. Sidi-Boumedine, M. Janier, K. Butterworth, S. Mcmahon, K. Prise, M.-T. Aloy, D. Ardail, C. Rodriguez-Lafrasse, E. Porcel, S. Lacombe, R. Berbeco, A. Allouch, J.-L. Perfettini, C. Chargari, E. Deutsch, G. Le Duc and O. Tillement, *Br. J. Radiol.*, 2018, **91**, 20180365.
13 P. Bouziotis, D. Stellas, E. Thomas, C. Truillet, C. Tsoukalas, F. Lux, T. Tsokatos, S. Xanthopoulos, M. Paravatou-Petsotas, A. Gaitanis, L. A. Moulopoulos, V. Koutoulidis, C. D. Anagnostopoulos and O. Tillement, *Nanomedicine*, 2017, **12**, 1561–1574.
14 C. Truillet, E. Thomas, F. Lux, L. T. Huynh, O. Tillement and M. J. Evans, *Mol. Pharm.*, 2016, **13**, 2596–2601.
15 W. Price and C. Orvig, *Chem. Soc. Rev.*, 2013, **43**, 260–290.
16 E. Gourni, C. Canovas, V. Goncalves, F. Denat, P. T. Meyer and H. R. Maecke, *PLoS One*, 2015, **10**, e0145755.
17 G. Patonay, J. Salon, J. Sowell and L. Strekowski, *Molecules*, 2004, **9**, 40–49.
18 L. Wang, J. Jin, X. Chen, H.-H. Fan, B. K. F. Li, K.-W. Cheah, N. Ding, S. Ju, W.-T. Wong and C. Li, *Org. Biomol. Chem.*, 2012, **10**, 5366.
19 D. Lhenry, M. Larrouy, C. Bernhard, V. Goncalves, O. Raguin, P. Provent, M. Moreau, B. Collin, A. Oudot, J.-M. Vrigneaud, F. Brunotte, C. Goze and F. Denat, *Chem.–Eur. J.*, 2015, **21**, 13091–13099.
20 N. Maindron, M. Ipuy, C. Bernhard, D. Lhenry, M. Moreau, S. Carme, A. Oudot, B. Collin, J.-M. Vrigneaud, P. Provent, F. Brunotte, F. Denat and C. Goze, *Chem.–Eur. J.*, 2016, **22**, 12670–12674.
21 V. Duhéron, M. Moreau, B. Collin, W. Sali, C. Bernhard, C. Goze, T. Gautier, J.-P. Pais de Barros, V. Deckert, F. Brunotte, L. Lagrost and F. Denat, *ACS Chem. Biol.*, 2013, **9**, 656–662.
22 A. M. Brouwer, *Pure Appl. Chem.*, 2011, **83**, 2213–2228.
23 C. J. Anderson and R. Ferdani, *Cancer Biother. Radiopharm.*, 2009, **24**, 379–393.
24 C. Truillet, P. Bouziotis, C. Tsoukalas, J. Brugière, M. Martini, L. Sancey, T. Brichart, F. Denat, F. Boschetti, U. Darbost, I. Bonnamour, D. Stellas, C. D. Anagnostopoulos, V. Koutoulidis, L. A. Moulopoulos, P. Perriat, F. Lux and O. Tillement, *Contrast Media Mol. Imaging*, 2015, **10**, 309–319.
25 G. Le Duc, S. Roux, A. Paruta-Tuarez, S. Dufort, E. Brauer, A. Marais, C. Truillet, L. Sancey, P. Perriat, F. Lux and O. Tillement, *Cancer Nanotechnol.*, 2014, **5**, 4.
26 L. Sancey, S. Kotb, C. Truillet, F. Appaix, A. Marais, E. Thomas, B. van der Sanden, J.-P. Klein, B. Laurent, M. Cottier, R. Antoine, P. Dugourd, G. Panczer, F. Lux, P. Perriat, V. Motto-Ros and O. Tillement, *ACS Nano*, 2015, **9**, 2477–2488.
27 F. Cusin, L. Fernandes Azevedo, P. Bonnaventure, J. Desmeules, Y. Daali and C. M. Pastor, *Basic Clin. Pharmacol. Toxicol.*, 2017, **120**, 171–178.
28 H. S. Choi, W. Liu, P. Misra, E. Tanaka, J. P. Zimmer, B. Itty Ipe, M. G. Bawendi and J. V. Frangioni, *Nat. Biotechnol.*, 2007, **25**, 1165–1170.
29 S. Luo, E. Zhang, Y. Su, T. Cheng and C. Shi, *Biomaterials*, 2011, **32**, 7127–7138.